Summer 1993

Absorption Imaging Studies on Intrinsic GaAs

John Samuel Kenney
Old Dominion University

ABSORPTION IMAGING STUDIES ON INTRINSIC GaAs

by

John Samuel Kenney

This Thesis Submitted to the Committee of
Old Dominion University in Partial Fulfillment of the
Requirements for the Degree of:

MASTER OF SCIENCE in ELECTRICAL ENGINEERING

OLD DOMINION UNIVERSITY

August, 1993

Approved by:

Dr. Karl Schoenbach

Dr. Vishnu K. Lakdawala

Dr. Ravindra P. Joshi

ABSTRACT

ABSORPTION IMAGING STUDIES ON INTRINSIC GaAs

John Samuel Kenney

Old Dominion University

Advisor: Dr. Karl Schoenbach

A diagnostic technique has been developed which allows recording of the temporal and spatial development of electric field structures in GaAs photoconductive switches. The optical method is based on the Franz-Keldysh effect. Measurements were performed with a Nd:YAG activation laser and a GaAs laser diode as the probe laser. At low applied voltages a 100 μm wide region of high electric field is seen at the cathode only. With increasing voltage strong domain like structures emerge at the anode also. A calibration measurement shows that the electric fields in these domains are well above 50 kV/cm. At a threshold voltage, current filaments were recorded which cause a permanent current flow, the lock-on current, and at extreme levels permanent damage of the sample.

ACKNOWLEDGEMENTS

My first expression of gratitude and appreciation is to Dr. Karl Schoenbach who overlooking my many faults has given me this chance to work in research and obtain my graduate degree. His willingness to communicate and fatherly guidance during my graduate career is much appreciated and will never be forgotten.

I would like to thank Dr. Vishnu Lakdawala for all ways being there to give advice and encouragement. He also has been very monumental in the administrative side of my graduate degree.

My thanks to Dr. Ravindra Joshi whose excellent teaching skills and willingness to explain beyond the call of duty has given me a greater interest and understanding in areas of applied physics that I previously did not think possible. Much appreciation goes to Dr. Ralf Brinkman, Dr. Herbert Eichhorn, Thomas Tessnow and Frank Peterkin for all there helpful discussions that have directly contributed to the completion of this thesis. Also the many undergraduate assistants past and present that have served as coworkers as well as friends.

To Randy Roush and especially David Stoudt I owe much for giving me the inspiration and vision to obtain my graduate degree. Dave has always challenged me through his example to push myself in attaining a high standard in both academics and work quality.

The continual encouragement and support from my parents in every endeavor that I have embarked on has been invaluable. Finally and most importantly I give all the credit to the Lord Jesus Christ. May my success and accomplishments be all to the glory of God.

TABLE OF CONTENTS

PAGE

LIST OF FIGURES

LIST OF PHOTOGRAPHS

CHAPTER 1

INTRODUCTION

1.1 Introduction

In recent years the field of photoconductive switching has progressed rapidly. The attractive features of this kind of switching as compared to other means such as gas discharge switches are electrical isolation of control and switching circuits, fast rise-times limited only by the activation source, and practically no jitter. However, even though the dielectric strength of the material is general on the order of several hundred kV/cm[1] the actual breakdown can occur at a much lower value possibly due to localized high fields at the contact region.[2] In order to optimize photoconductive switches with respect to hold-off voltage, the temporal and spatial nature of these high field regions need to be known. At the present only one method exists for the evaluation of surface fields on such a switch through electro-optic means[3]. This method indirectly gives the distribution of internal fields. The topic of this thesis is the development of a diagnostic technique to directly analyze the behavior of fields through band-edge absorption in the bulk of the switch.

1.2 Materials of Interest

The most common material used in photoconductive switching is GaAs due to its low leakage currents and high electron mobilities. Semi-insulating GaAs has

a very high resistivity and would lend itself well to very high hold-off voltages utilized in high-power photoconductive switching. Thus the importance in understanding the behavior of the switch at high fields can be realized.

1.3 Lock-on

Two different modes, the linear and nonlinear modes exist that switches can operate in. The linear mode is characterized by the linear increase of current with the activation intensity. For the nonlinear mode the phenomenom of lock-on is observed when the applied voltage reaches a critical value, V_{cr}[4]. At and above this value the switch is unable to recover to its initial hold-off voltage after the termination of the activation source. Instead the voltage is "locked-on" to a constant value, corresponding to an average electric field strength in the range of 4 to 12 kV/cm[5].

Schematically the difference between lock-on and operation in the linear regime is shown in Figure 1.1. The first current and voltage waveforms are what would be expected when $V_0 > V_{cr}$. With activation, the voltage drops and current rises to a value determined by conduction of the switch and the external circuit. With the removal of the activation source, the switch recovers and the voltage returns to the initial value V_0. Operation above the critical value V_{cr} is shown in the second current and voltage waveform. After the removal of the activation source the voltage returns to V_{LO}, the lock-on voltage. For both scenarios the switch is initially in a highly resistive state with very small dark currents. It has been observed that the

amplitude of the lock-on current does not seem to be dependent on the intensity of the activation source but more directly on material dependent transport processes occurring at high fields[4].

Figure 1.2 shows the typical current traces for the linear and the nonlinear (lock-on) mode of current conduction. The total time of the applied voltage is 300 ns and is indicated with the beginning and ending arrows. The activation laser occurs 100 ns after this and for the linear mode immediately decays back down to a negligible current. For the nonlinear mode, after an initial decay the current is reestablished at a different level and extinguished only with the decay of the applied voltage.

A possible explanation for the steady state behavior is based on the strongly nonlinear dark current in semiconductors containing deep centers and ohmic contacts which allow double injection[4]. The transition into lock-on can be seen in Figure 1.2 which schematically shows the three different I-V curves possible in a switching cycle: i) the transient dark current, ii) the steady-state dark current, and iii) the induced current. The following switching scenarios demonstrate this concept.

The same load resistor is used for both but with different initial voltage V_0 characterized by the two load lines I and II. For the first case, the switching cycle begins with an initial voltage $V_{0I} < V_{cr}$ and a small dark current at point a_I. The cycle then moves along load line I to a low resistive state, b_I due to the irradiation. After the termination of the irradiation, the charge carriers recombine, the switch opens, and the cycle ends back at point $a_I = c_I$. No lock-on is observed for this case.

In the second case with load line II, the initial voltage V_{0II} is greater than the critical value V_{cr}. In the initial off state, the cycle begins at point a_{II} on the transient dark current curve. This current is smaller than the steady-state dark current because we have not allowed enough time to reach the steady-state dark current, which has a voltage dependent onset time[6]. In actuality, a_{II} is moving slowly along the load lime with a time constant determined by trap filling processes shown by the dashed line. This scenario would be for the case of a pulsed voltage where sufficient time has not been allowed before the application of the irradiation. At the time of irradiation the traps are filled quickly and point b_{II} is reached on the load line. With the termination of the irradiation, the load point moves to the trap-filled value on the dashed line coming to rest at the steady-state dark current value c_{II}.

This curious characteristic has been observed in different types of GaAs, InP and recently in diamond. Generally lock-on is considered detrimental due to the devolopement of filamentary currents[7] and the self destructive nature of operation in this mode. Although this model explains the steady state behavior of lock-on, it does not give us information on the physical process leading to double injection.

1.4 Surface Electric Field Probing (Electro-Optic)

An electro-optic imaging technique has so far been used by a research group in Rochester NY, to monitor rapid variations of the surface electric field between the contacts on a photoconductive switch[3]. The surface electric field is related to the internal field in the bulk because the tangential component of the electric field is

continuous across a dielectric interface. Since the internal field is modified by the presence of the carriers in the gap, the surface field imaging through electro-optic means can be used to investigate the behavior of charge carriers within the switch.

The setup for this technique is shown in Figure 1.3. A large area sampling beam interrogates the electric field over a wide surface. The polarization of the sampling beam interacts with the surface electric field through an electro-optic crystal located on the switch surface. In response to the field the crystal changes its birefringence rotating the polarization of the probe beam. The probe beam is then imprinted with an optical analog of the spatial electric field distribution. The back reflected beam at the polarizer directs only the light that has been rotated to a camera. By comparing the intensity at the camera with and with no voltage applied, the rotation due to the electric field can be determined. This sampling occurs only when the probe pulse is present resulting in a snapshot of the instantaneous electric field during different phases of photoconductive switching.

1.5 Bulk Electric Field Probe (Band-edge Absorption)

A direct means of observing the internal field structures utilizes band-edge absorption. The absorption of insulators and semiconductors can be effectively shifted by the influence of electric fields (Franz-Keldysh effect), magnetic fields, changes in temperature, pressure and carrier density. This shift in the absorption can be very drastic for a direct band-gap material such as GaAs as shown in Figure 1.4. The effect is such that the local absorption of light at the band-gap increases with a

local increase in the value of these parameters. For photoconductive switches with only a voltage applied, the effects of electric fields and temperature can be expected to dominate.

Under a pulsed voltage bias, the photoconductive switch is activated. Then a probe beam with a wavelength at the band-edge illuminates the bulk of the material. Due to local fields and temperature variations, the absorption of the probe beam is locally modulated and the transmitted light is then recorded with a camera. The temporal resolution is determined by the probe laser pulse width. The spatial resolution is limited by diffraction on the order of the wavelength of the probe laser and the resolution of the camera.

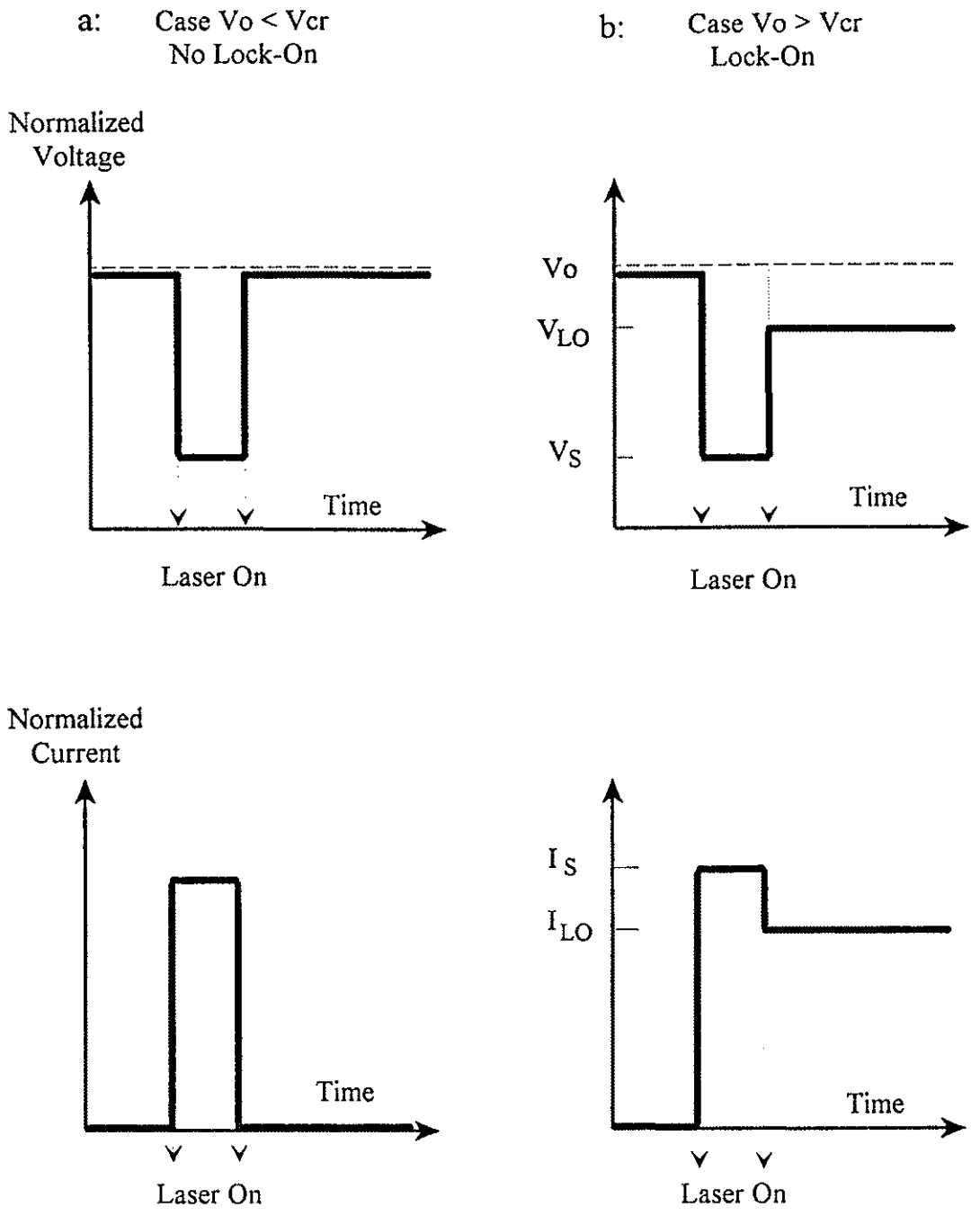

Figure 1.1 Idealized voltage and current representation of the linear mode (a) and the nonlinear or lock-on mode (b) of activation.

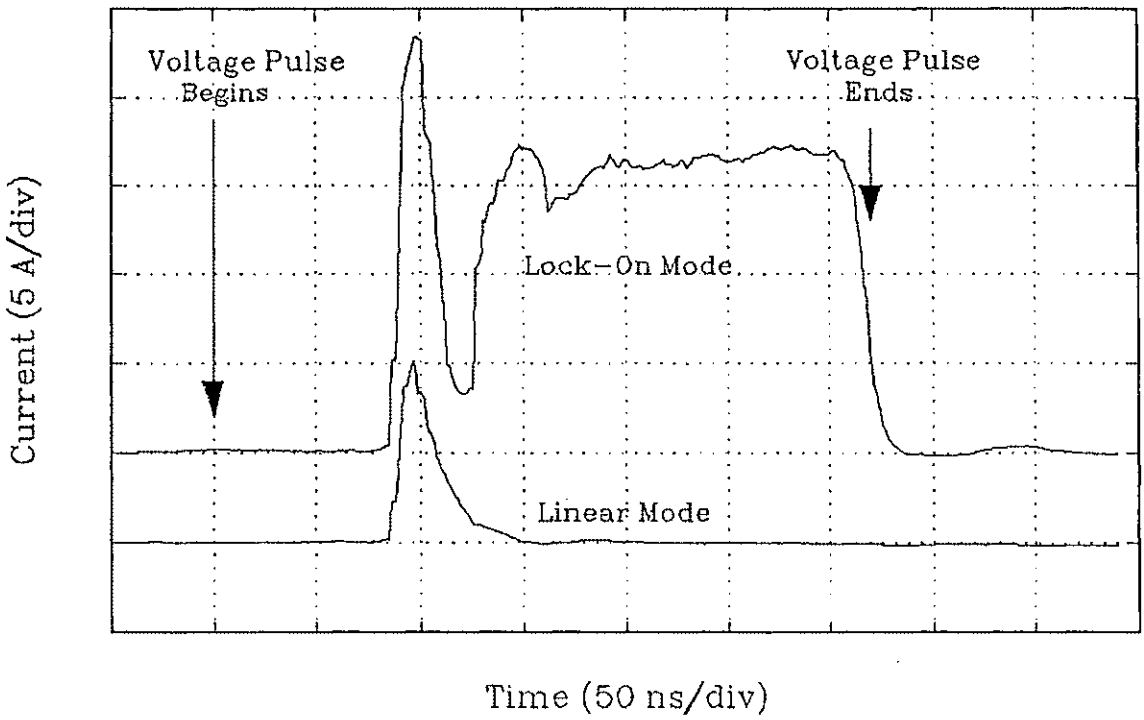

Figure 1.2 Typical scope current traces for the linear and nonlinear mode of current conduction.

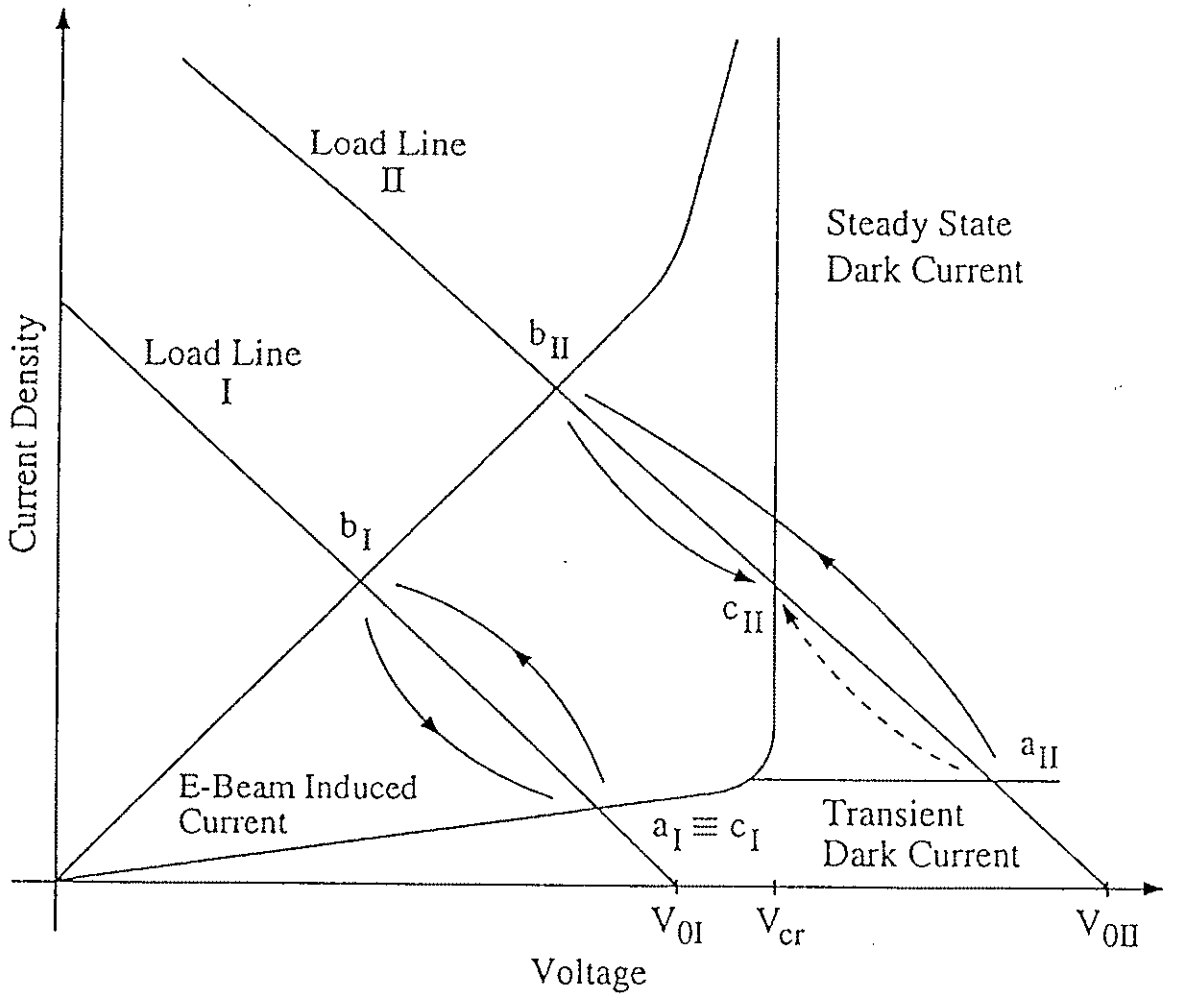

Figure 1.3 Schematic representation of the lock-on switching cycle.

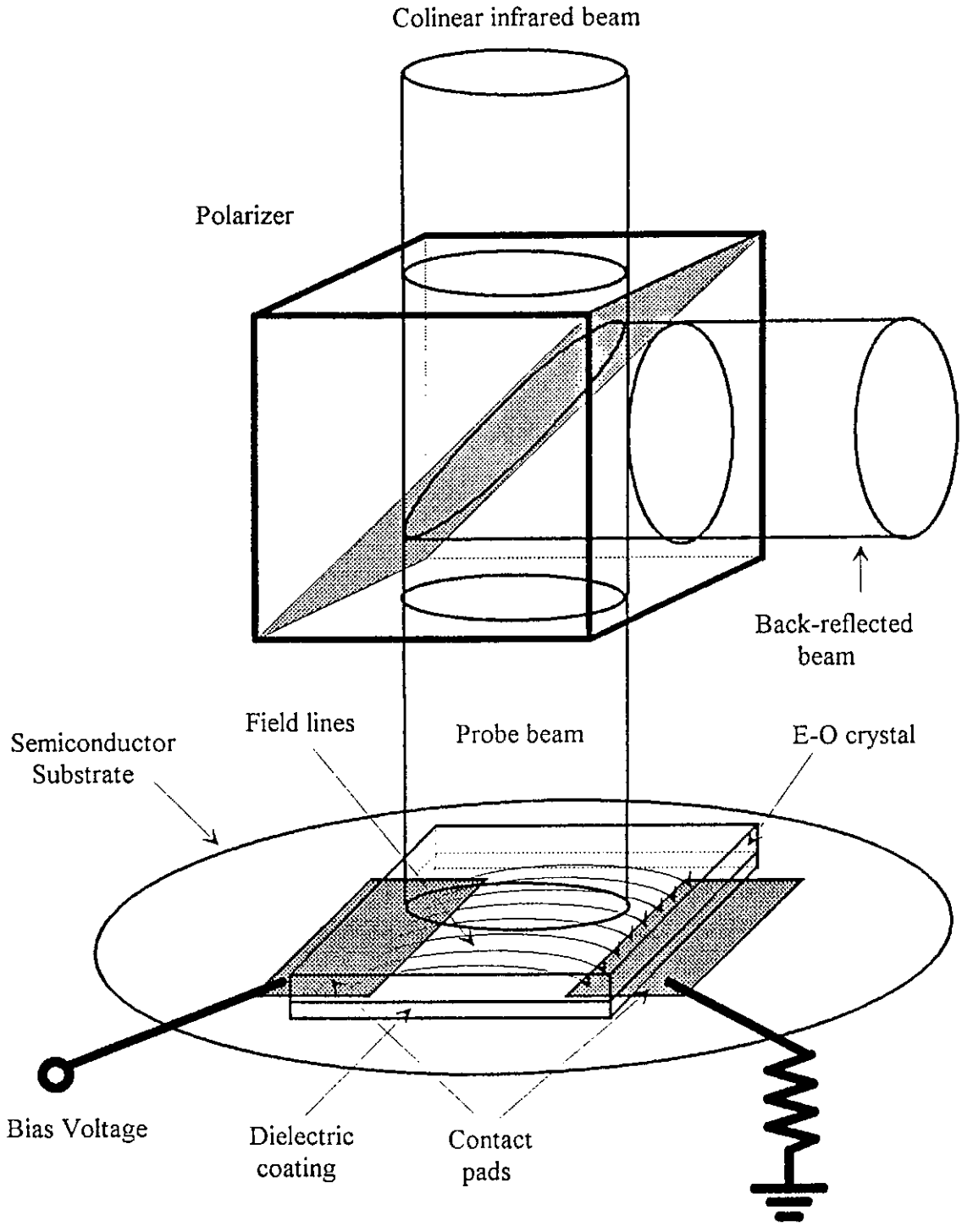

Figure 1.4 Electro-optic surface field probe setup.

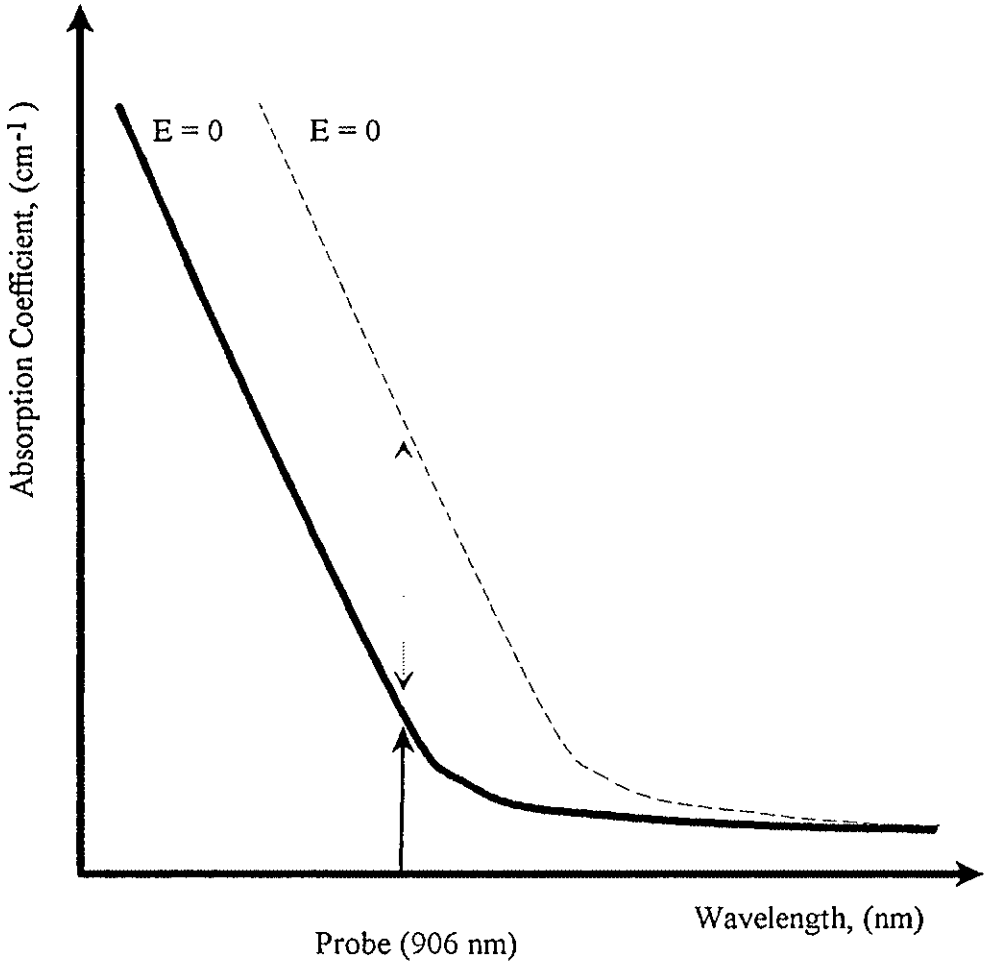

Figure 1.5 Change in the absorption coefficient with a shift in the band-edge due to the application of a field.

CHAPTER 2

THEORY

2.1 Absorption

GaAs is a type III-IV direct band-gap semiconductor that exhibits a strong change in absorption at it's band-edge. The absorption of light in a material decays exponentially with distance x. At each interface there will be a reflected component and a transmitted component. The total transmission or reflection will then be the summation of all these as shown in figure 2.1. Taking into account these multiple reflections and by using a Taylor series simplification we obtain equation 1.

$$I(x) = \frac{I_o\,(1 - R)^2\, e^{-\alpha x}}{1 - R^2\, e^{-2\alpha x}} \qquad (1)$$

Where: I_o is the initial intensity,

R is the reflection coefficient,

α is the absorption coefficient,

and x is a distance.

2.2 Effect of External Parameters on the Absorption-Edge

There are several external parameters that are known to cause a shift in the absorption edge of semiconductors and insulators. These are electric and magnetic fields, pressure, temperature and large concentrations of charge carriers.

Pressure can be either uniaxial or hydrostatic and effects the potential energy of all the levels. Temperature can effect the population of various states and the potential of the levels through the internal pressure changes. Magnetic fields can cause Landau splitting of all the states in the conduction and valence bands and a Zeeman splitting of impurity and exciton states. Electric fields can polarize the lattice and at extreme levels induce the Stark effect, a splitting of levels. But most importantly the Franz-Keldysh effect effectively broadens all the states.[8]

The Franz-Keldysh effect was so named after theoretical work done concurrently by two scientists, W. Franz and L.V. Keldysh back in 1958.[9,10] The effective broadening of states or shifting of the band-edge with high electric fields results in increased absorption. The result is that a photon-assisted tunneling through the energy barrier of the forbidden gap becomes more possible.

For the photoconductive switches operating on very short time scales the amount of energy deposited is minimal and significant temperature changes would not be observed. Also no magnetic field or pressures effects are expected since none are applied. The switch current is generally so small that its magnetic field can also be neglected. This then leaves the Franz-Keldysh effect as the predominant effect that would be present during photoconductive switching. The theory involved with this will be presented in more detail in the following section.

2.3 The Franz-Keldysh Effect

When an electric field is applied, there is a greater probability of finding an electron or hole inside the forbidden gap. This results in an exponential broadening

of the states into the gap by an average deviation which depends on the applied E-field. The way this occurs starts with a tilting of the band-edges in the presence of an applied field. An electron moving inside a band with kinetic energy *qEx* has a momentum that is an energy of hν. If this electron were to move away from the band-edge into the gap maintaining a constant total energy, then it's kinetic energy becomes negative. The corresponding momentum then becomes imaginary and the wave function of the electron in the gap is represented by a damped wave. The probability of finding an electron inside the forbidden gap is then described by an exponentially decaying function: Ue^{-ikx}. This probability decreases away form the band-edge according to equation 2.

$$e^{-\left(\frac{|E - E_e|}{\Delta E}\right)^{3/2}} \qquad (2)$$

Where: E is the energy at point x,

E_e is the energy of the band-edge at x,

ΔE is a parameter with a dependence of equation 3 on the E-field according to:

$$\Delta E = \frac{3}{2} (m^*)^{-1/3} (q \hbar \mathscr{E})^{2/3} \qquad (3)$$

Where: m^* is the effective electron or hole mass,

q is the charge,

$\hbar$ is Planck's constant,

$\mathscr{E}$ if the applied electric field.

The quantumechanical treatment that leads to these solutions can be found in Appendix A.

Graphically the process is shown in figure 2.2. Shown is the tilted conduction and valence band-edges with the probability function for holes (solid line) and electrons (dashed line) superimposed on them. In the respective bands the probability function is seen as oscillatory and exponentially decreasing in the forbidden gap. For an unassisted tunneling process the valence electron must tunnel through a triangular barrier of height E_g, and thickness of value d as shown in equation 4.

$$d = \frac{E_g}{q\,\mathscr{E}} \tag{4}$$

As the E-field is increased, the tunneling distance is reduced and the overlap of the wave functions are increased. The wave functions describe the probability of finding and electron at a given location. When a photon of energy $h\nu$ is added (figure 2.b), this is equivalent to reducing the barrier thickness by a value of d' in equation 5.

$$d' = \frac{(e_g - h\nu)}{q\,\mathscr{E}} \qquad (5)$$

The further increase in the overlap of the wave function makes the tunneling transfer more probable.[12] With either increasing photon energy or increasing E-field the tunneling process becomes more likely.

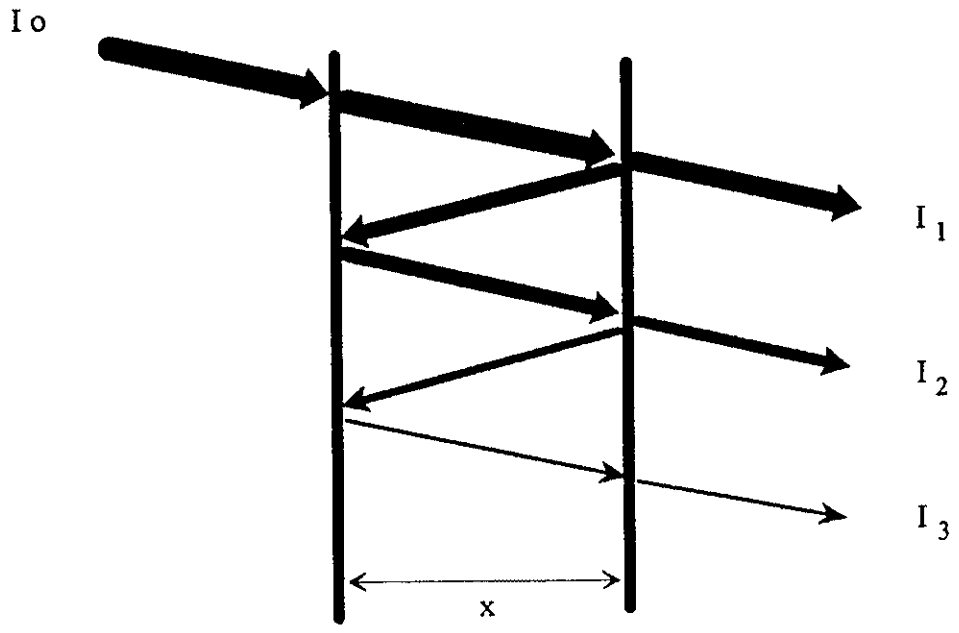

$$I(x) = I_1 + I_2 + I_3 + \ldots$$

Figure 2.1 Summation of transmission and reflection components that give rise to the absorption coefficient.

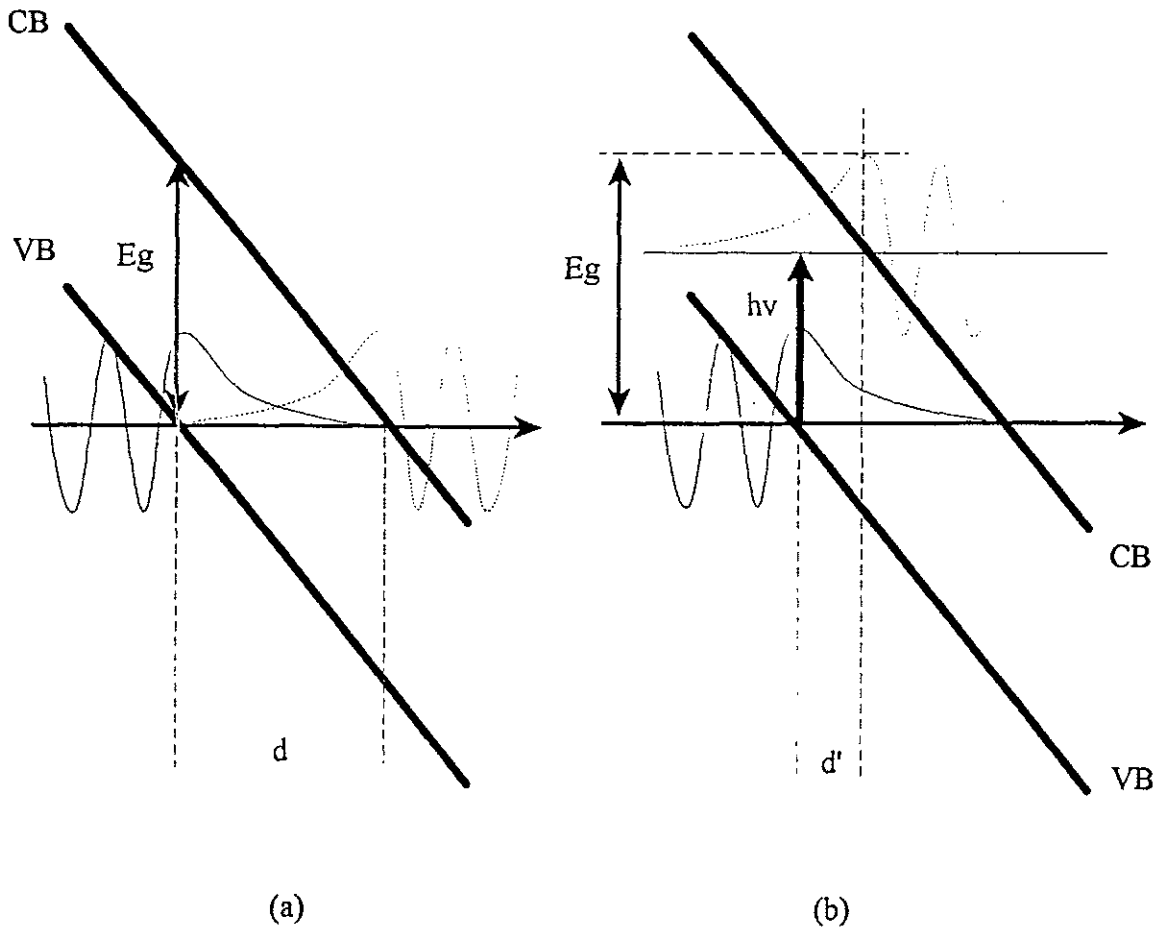

Figure 2.2 Electron tunneling (a) without change in energy, (b) with photon absorption.

CHAPTER 3

EXPERIMENTAL SETUP

3.1 Experimental Setup and the Four Main Components

The experimental setup consists of four main sections that are individually discussed. First is the GaAs switch along with the biasing and diagnostic circuit. Second is the activation laser. Third is the probe laser, and fourth is the image recording diagnostic setup. The results obtained with this experimental setup will be presented in the following chapter.

The first part is the GaAs switch itself. The material used was semi-insulating GaAs with a resistivity in the Mega Ω-cm range. Contacts were in a coplanar configuration. Contacts were made by evaporating AuGe through a mask which were then annealed to the surface at 150°. Copper strip leads were attached using silver epoxy which resulted in ohmic contacts. This configuration and the typical dimensions are shown in figure 3.1.

The switch was pulse biased using a transmission line pulser. The cable discharge is capable of generating a rectangular voltage pulse with a rise-time of 20 ns up to several kV for a duration of 300 ns into a matched load of 50 Ω. The switch is then placed in parallel or series to the 50 Ω load resistor. Current measurements are made using a 2.4 Ω CVR on the ground side of the switch.

The activation laser is a Nd:YAG laser with a wavelength of 1064 nm. The laser was a Spectra Physics DCR-11 generating MW pulses with a FWHM of 7 ns. The intensity was attenuated using various neutral density filters and beam spliters.

The probe beam is a stacked laser diode array from Laser Diode Inc. which has a pulse duration (FWHM) of 30 ns and a peak power of 60 W. The spectral width at the center wavelength of 906 nm is 3.5 nm. The wavelength is stabilized using a temperature controller from Light Control Instruments Inc. (model 320). The output wavelength can be varied by 0.3 nm/°C.

The image recording device is a high sensitivity CCD digital camera from Electrim Corp. (model # EDC-1000) which operates as an open shutter IR-camera. The spectral range is from 400 nm to 1100 nm with a pixel resolution of 192 (horizontal) by 165 (vertical). Images can be down loaded to a PC for storage and image processing.

Spectral filtering was used to maintain image clarity and accuracy. The spectral filter was a low-pass filter with a cutoff wavelength at 950 nm. The purpose of using this was to prevent any scattered Nd:YAG radiation from reaching the CCD camera.

The complete experimental setup is shown in figure 3.2. The activation laser light was first passed through a neutral density filter (NDF) to reduce the intensity. Then the beam was focussed (L-2) onto a quartz homogenizing rod (HO-2). This homogenized beam was then shown on the switch at an angle of 45°. Energy of the incident radiation was measured by placing a mask with an opening the same size as

the illuminated switch area at the same position as the switch. The transmitted radiation was then recorded using a Scientec thermal detector. The typical energy measured for the activation source was 0.5 mJ/cm^2.

The relative timing between the two lasers and the voltage pulse was controlled by a four channel Stanford Research digital delay and pulse generator (Model DG535) which had a delay resolution of 5 ps. Photocurrent waveform acquisition was accomplished using a Tektronix transient digitizer (Model 7912) which had a 700 MHz bandwidth vertical amplifier. All of the control equipment was housed in a Faraday cage for electrical noise discrimination.

3.2 Calibration Setup

The calibration set up essentially used the same setup as previously described with a few minor changes. Since we wanted to observe the uniform darkening between the contacts due to the Franz-Keldysh effect no activation laser was used. The applied voltage pulse was 25 ns, on the order of the pulse width of the probe diode.

The calibration experimental setup is shown in figure 3.3 and was essentially a 50 Ω transmission line pulser. An 8 foot cable length was chosen to deliver a 25 ns FWHM pulse switched through a GaAs photoconductive switch. The pulsers photoconductive switch was activated using the Nd:YAG laser which resulted in a rise time of 12 ns. The cable between the pulser and the experimental setup was chosen to be 24 feet so that in the case that the load was not matched, the resulting

reflection would occur much later in time. For a matched load, the system would deliver the characteristic 1/2 the charge voltage. The shape of this pulse is shown in figure 4.2 as a solid line along with the probe profile and the current.

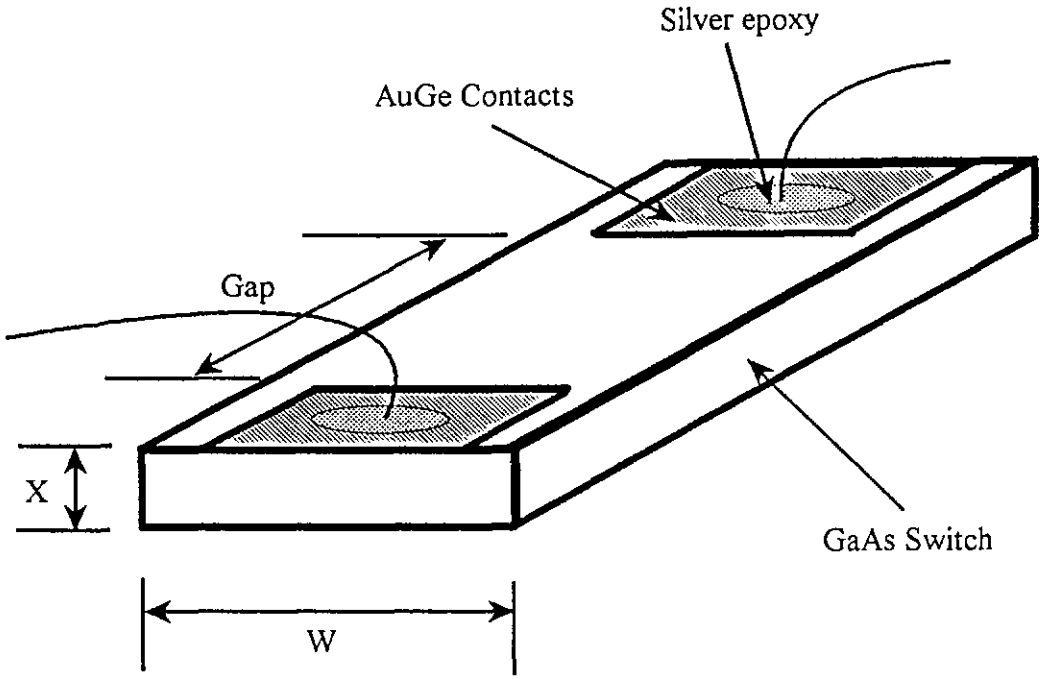

W = 5.0 mm

X = 0.5 mm

Gap = 2.0 mm

Figure 3.1 GaAs switch with coplanar AuGe contacts showing typical dimensions.

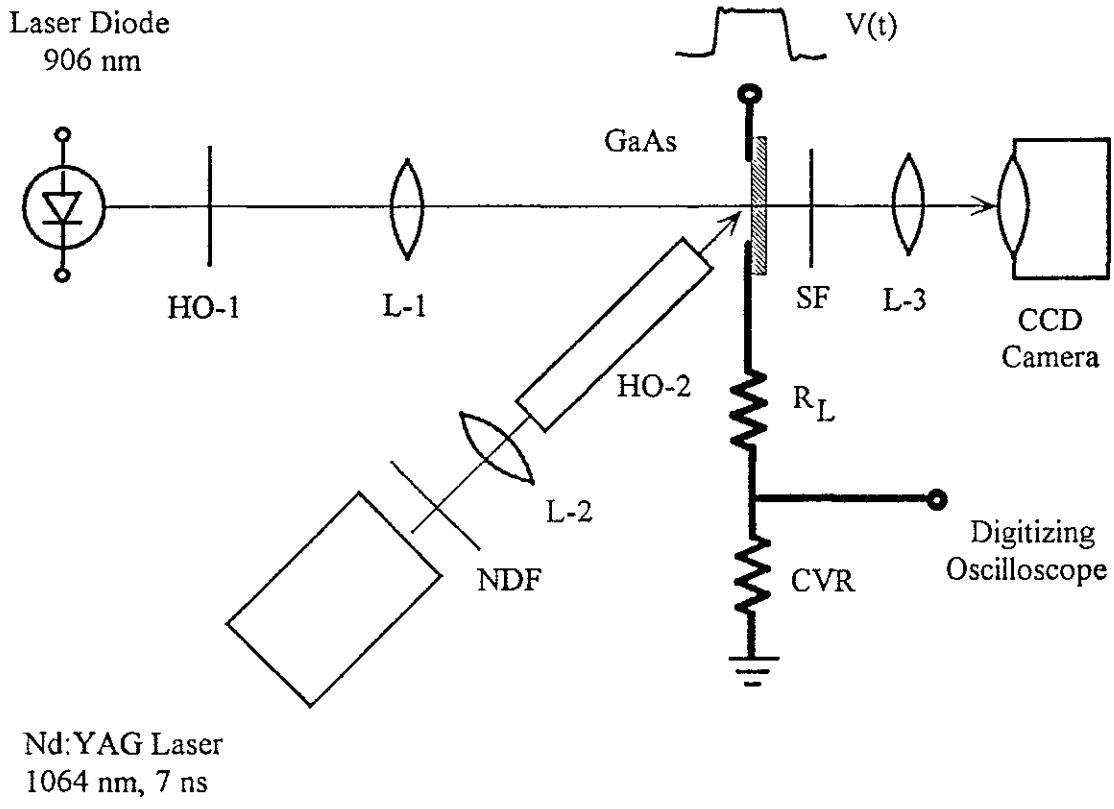

Figure 3.2 Experimental setup for the absorption imaging studies.

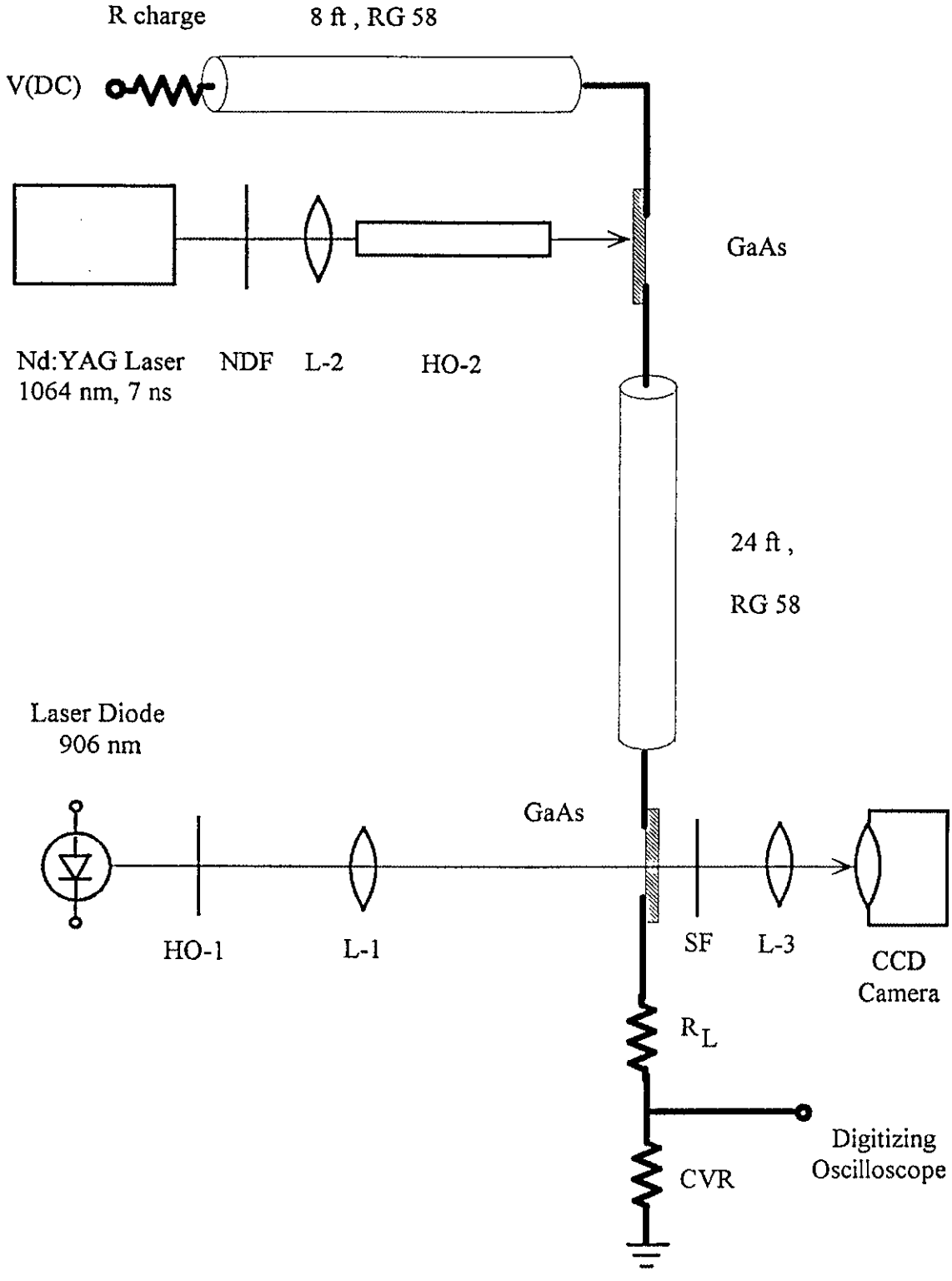

Figure 3.3 Experimental setup for the calibration measurements.

CHAPTER 4

EXPERIMENTAL RESULTS

4.1 System Performance

Figure 4.1 shows a reference photo of a typical planar geometry switch. Seen on either sides as dark areas are the contacts and the illuminated area between as the bulk of the material. The reference photo is taken with no voltage applied and no activation laser.

4.2 Calibration Results

In order to relate the magnitude of electric field with the electro-absorption in the sample the uniform change in absorption due to an applied electric field was measured. No activation laser was used so that the conducted current was negligible and temperature effects would not be present. The applied voltage pulse had a FWHM of 25 ns almost matching the probe diode lasers FWHM of 30 ns. The oscilloscope trace of these two and the current waveform are shown in figure 4.2. The displacement current was in the milliamp range.

With an applied voltage of 7.2 kV (31 kV/cm) and a probe wavelength of 908 nm, a slight uniform darkening between the contacts is observed. Figure 4.3 (a) shows a reference photograph with no voltage applied and (b) shows the uniform darkening at 31 kV/cm. Figures 4.3 (c) and (d) are the image processed difference

pictures where the respective photos have been subtracted from the reference photo (a). Keeping the voltage the same and changing the wavelength to 902 nm, closer to the band-edge, the uniform darkening became more evident as seen in figure 4.4 (b) and the corresponding difference photo (c). Increasing the field to 9.9 kV (42 kV/cm) the absorption became stronger as shown in figure 4.5 (b) and the difference photo (b).

4.3 Results with Semi-Insulating GaAs

The temporal development of the absorption pattern at low illumination and applied voltage for a switch operating in the linear range is shown in figure 4.6. The applied voltage is 1.25 kV corresponding to an average electric field of 5.4 kV/cm. The pictures were taken at various times before (a), during (b) and after (c) the photoactivation of the switch. The switch was also probed after the voltage was removed (d) in order to determine the time it takes to fully recover to its original state. The first picture (fig. 4.6a) shows the absorption pattern of the switch after voltage was applied but before laser activation. There is no observable absorption pattern. During or immediately after laser activation a well defined absorption layer of about 100 μm thickness develops at the cathode (fig. 4.6b). Also mushroom like structures begin to emerge at the electrodes. The cathode layer disappears completely after the voltage is removed, as seen in figure 4.6c taken 200 ns after the voltage pulse. Remaining is the mushroom like structure, which is visible for over 10 μs (Fig. 4.6d). The cathode layer can be better seen in figure 4.7c, which is an

image processed replica of figure 4.7a. This figure was obtained by subtracting the absorption pattern of the unbiased switch (fig. 4.6a) from the distribution in figure 4.6b. Figure 4.7d is the image processed replica of figure 4.7b where the disappearance of the cathode layer is obvious.

An applied voltage of 2.75 kV, corresponding to an average electric field of 12 kV/cm, causes the switch in over 90% of the shots to transit into the lock-on state at current density threshold of 900 A/cm^2. The voltage across the switch when this state is established was measured as 1.4 kV $\pm$0.3 kV, which corresponds to an average electric field of 6 kV/cm with a statistical deviation of $\pm$20%. Figure 4.8, and 4.9 shows absorption patterns for the relatively rare case that lock-on was not obtained at an applied voltage of V = 2.75 kV. Figure 4.8a was obtained 40 ns after photoactivation and (b) is the difference photo from the reference. Figure 4.9 was obtained 180 ns thereafter and the corresponding difference photo is (b). At these voltages the absorption pattern differs drastically from that observed at lower voltage (Fig. 4.6). Absorption structures are developing after laser activation not only at the cathode but also at the anode. The structure at the cathode is much more complex than in the low voltage case and the absorption bands reach further into the gap. The cathode pattern varies from shot to shot and stays as long as the voltage is applied. The pattern in the anode region is relatively stable, that means that the principal features are about the same for consecutive shots.

When the switch transits into the lock-on state there is always a luminous filament visible. The filament emission, which contains radiation at the same

wavelength as the probe laser, creates a time integrated image on the CCD-camera screen and is therefore superimposed to any of the time resolved lock-on absorption patterns. Figure 4.10a and b shows the absorption structure of the switch before the lock-on current begins to flow, but after the laser activation. After the onset of the permanent current the field structure disappears (Fig. 4.11a,b). The filament seems to sweep out the high field domains. Dark spots inside the filament indicate thermal dissipation of energy which can lead to permanent damage, particularly at the contacts. The dark region was found to increase with every filamentary discharge passing through this area.

Figures 4.12, 4.13, and 4.14 show that reducing the intensity of the light activation at constant applied voltage causes the structure in the anode region to fade away. Also seen is that with lower levels of illumination the complexity of the absorption patterns reduces to a well defined anode and cathode region (fig 4.13a). For intensities below 3 $\mu J/cm^2$ these regions disappeared completely (fig. 4.12b). It was also observed that the onset of filamentation was shifted to higher voltages when the intensity was reduced, showing that the threshold voltage for the lock-on effect can be increased by lowering the light level of the activating light source. The current density threshold for lock-on correspondingly varied from 880 A/cm^2 to 1000 A/cm^2.

In a similar fashion figures 4.15, 4.16, and 4.17 were taken at a constant illumination while reducing the applied voltage. At the lower voltage (fig. 4.15 a,b) only a cathode absorption layer is observed but at the higher voltages both the anode

and cathode regions appear. Figure 4.17 a and b are both taken at an applied voltage of 2.5 kV where one shows the luminous filament and the other does not.

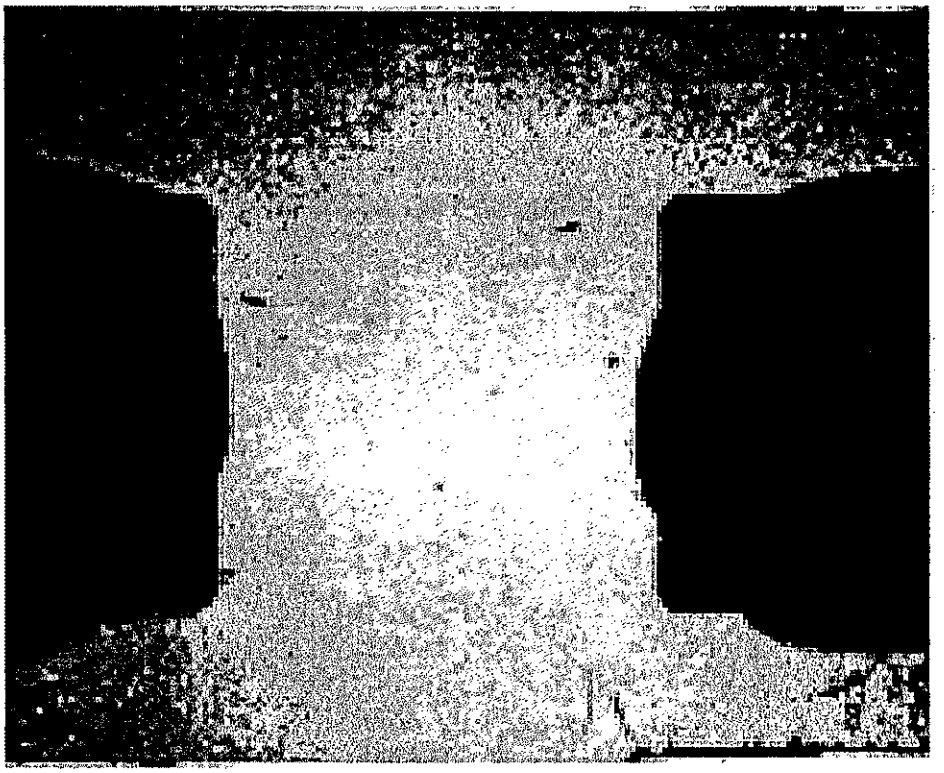

Figure 4.1 Reference photo of the planar geometry switch. In this and all subsequent figures the anode contact is on the left side of the switch.

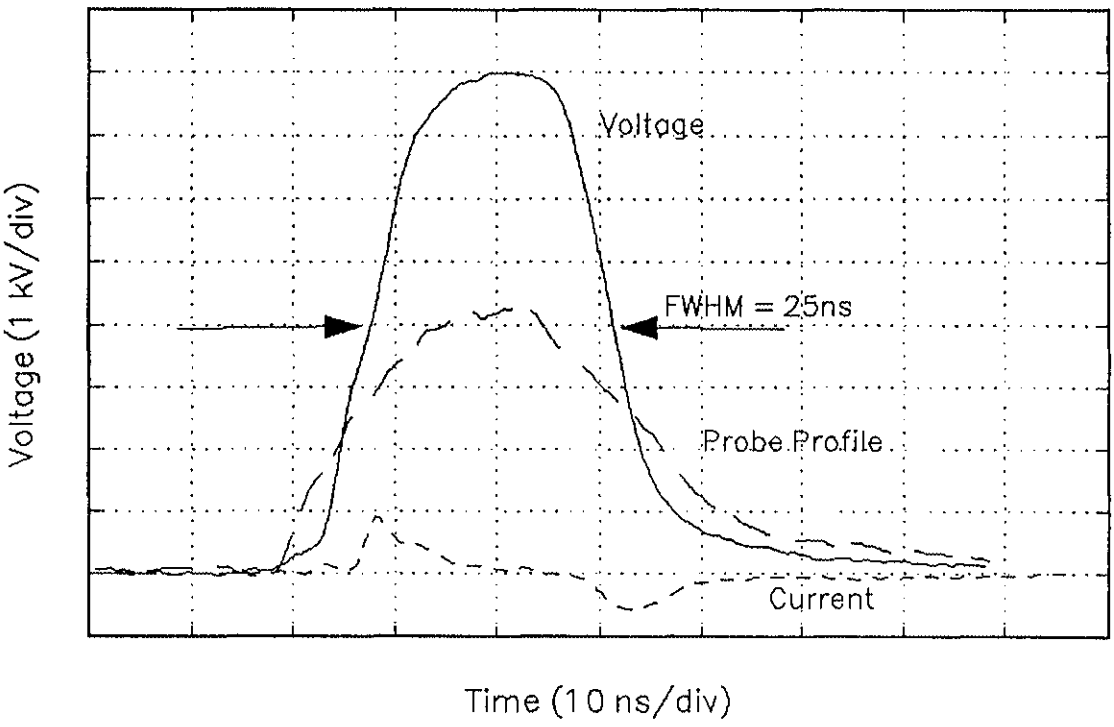

Figure 4.2 Scope traces of the 25 ns voltage pulse, current and the laser diode probe profile.

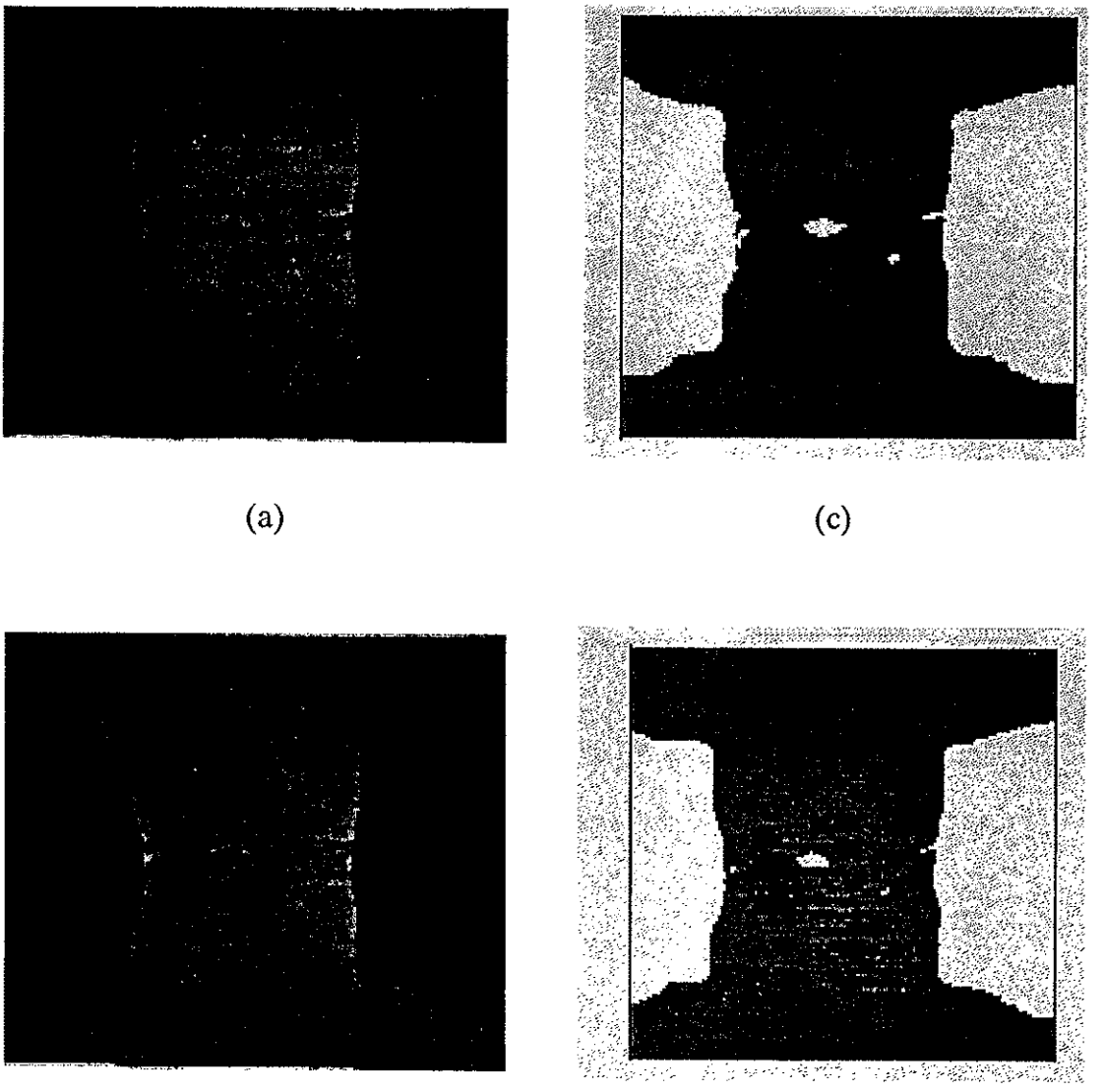

(a) (c)

(b) (d)

Figure 4.3 Reference photograph (a) taken with no voltage applied and (b) with an applied voltage of 7.2 kV (31 kV/cm) showing uniform darkening between the contacts. Photograph (c) and (d) are the image processed difference photos of (a) and (b).

(a)

(b)

(c)

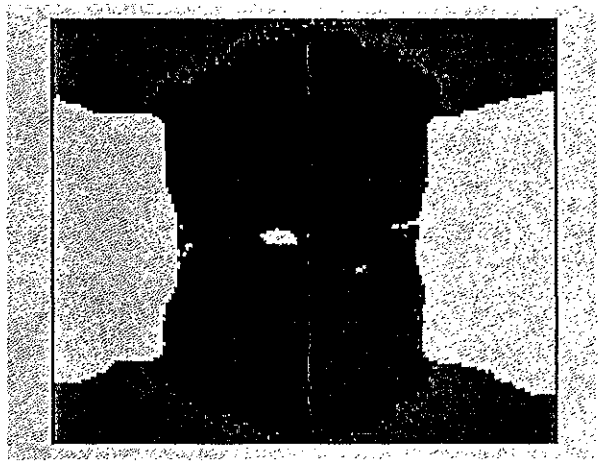

Figure 4.4 Reference photo (a) with calibration (b) and difference (c) photograph taken with the probe wavelength at 902 nm for an applied voltage of 7.2 kV (31 kV/cm).

(a)

(b)

(c)

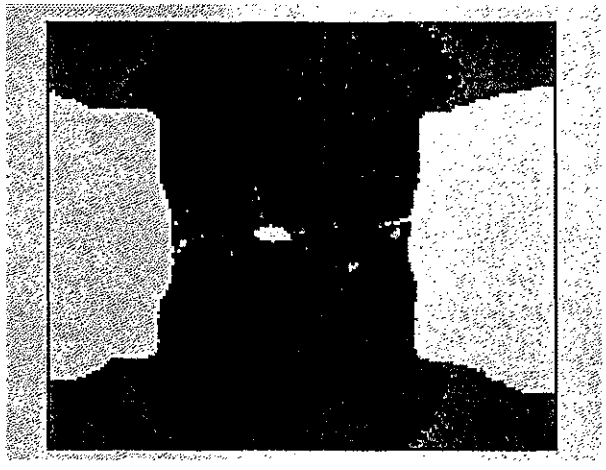

Figure 4.5 Reference photo (a) with calibration (b) and difference (c) photograph taken with the probe wavelength at 902 nm for an applied voltage of 9.9 kV (42 kV/cm).

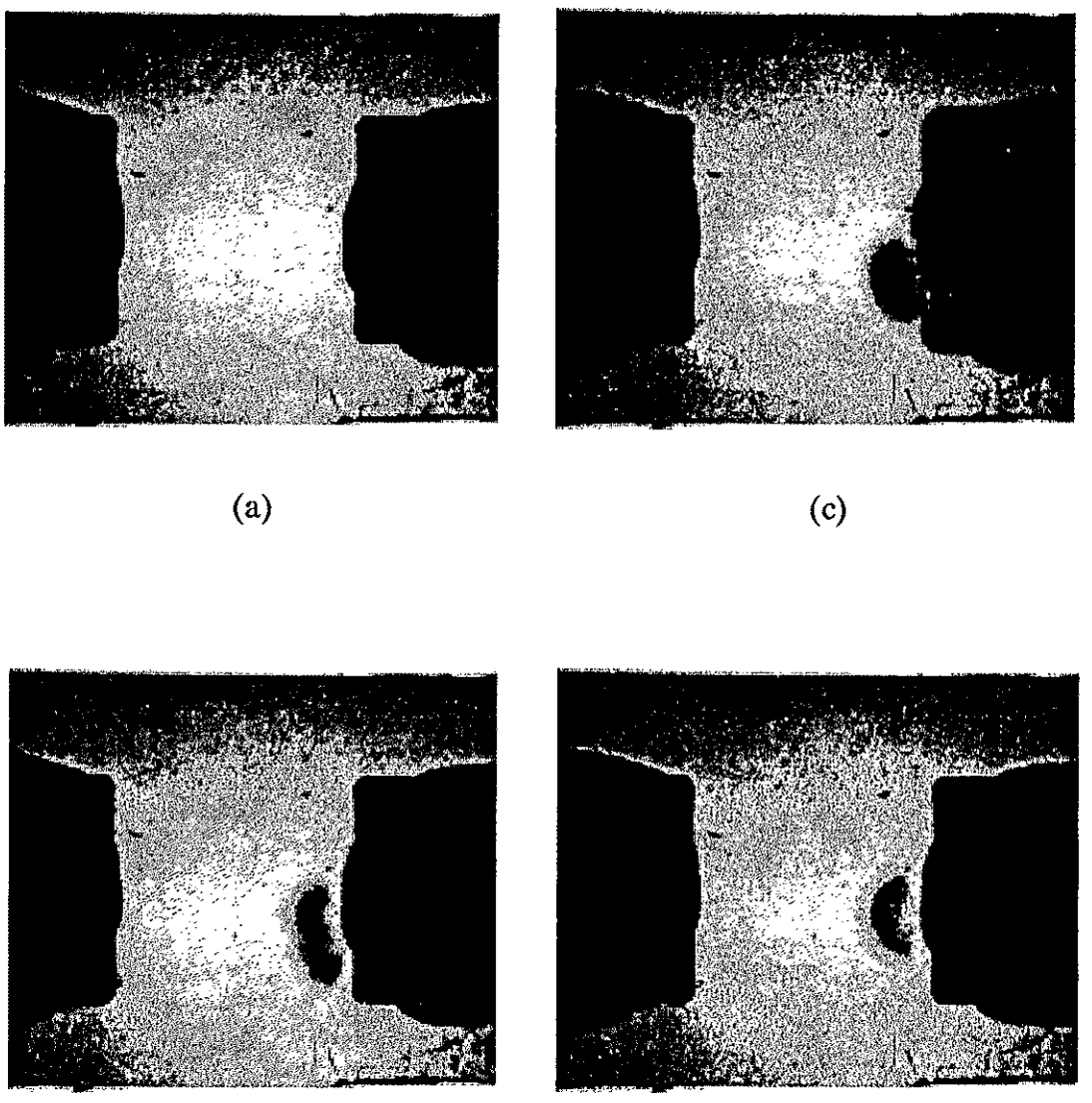

Figure 4.6 Variation of absorption structures with time at low illumination and applied voltage (1.25 kV). Pictures are probed at: (a) 50 ns, (b) 200 ns, (c) 550 ns, and (d) 10 μs after the rise of the voltage pulse.

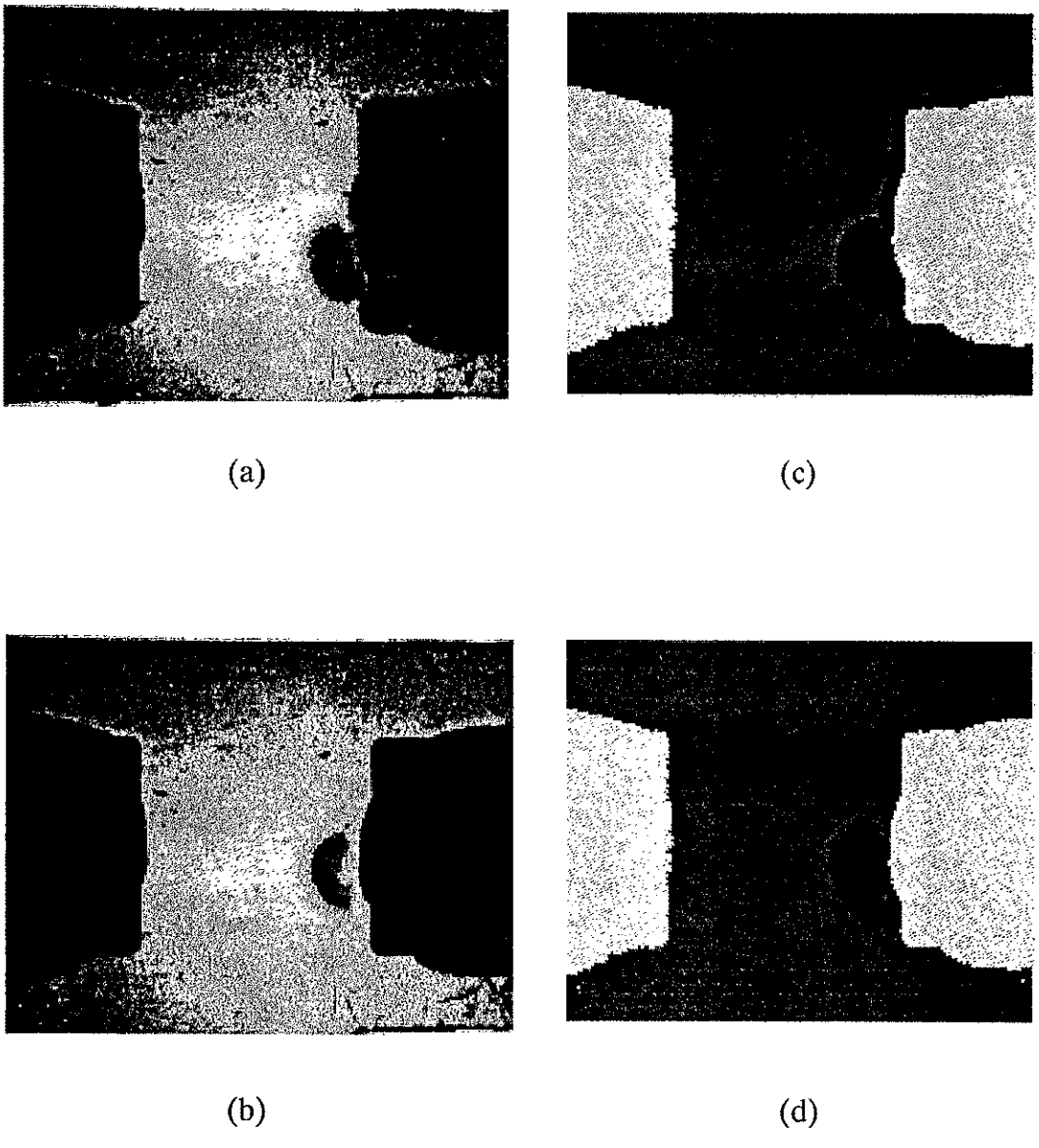

(a) (c)

(b) (d)

Figure 4.7 Variation of absorption structures from previous page (a) and (b) and there image enhanced difference photos (c) and (d).

(a)

(b)

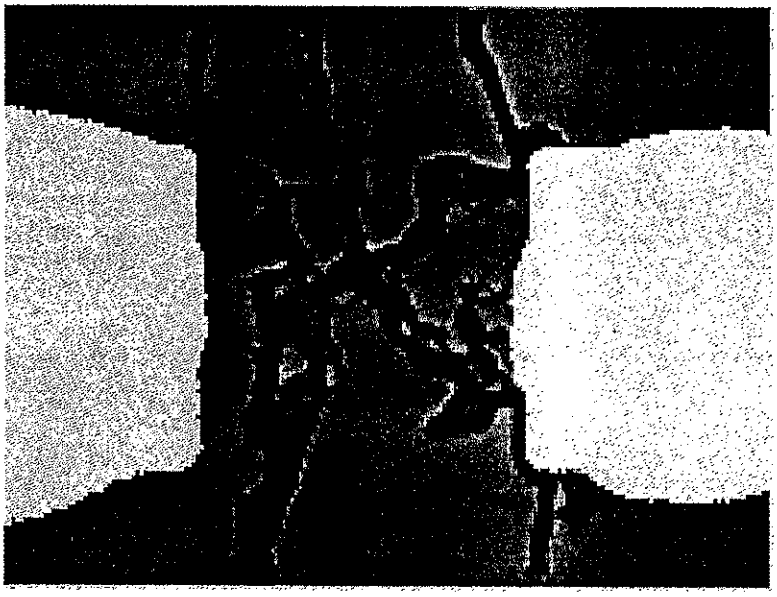

Figure 4.8 Absorption patterns at an applied voltage of 2.75 kV (a) probed 40 ns after laser activation and the corresponding image processed difference photo (b).

(a)

(b)

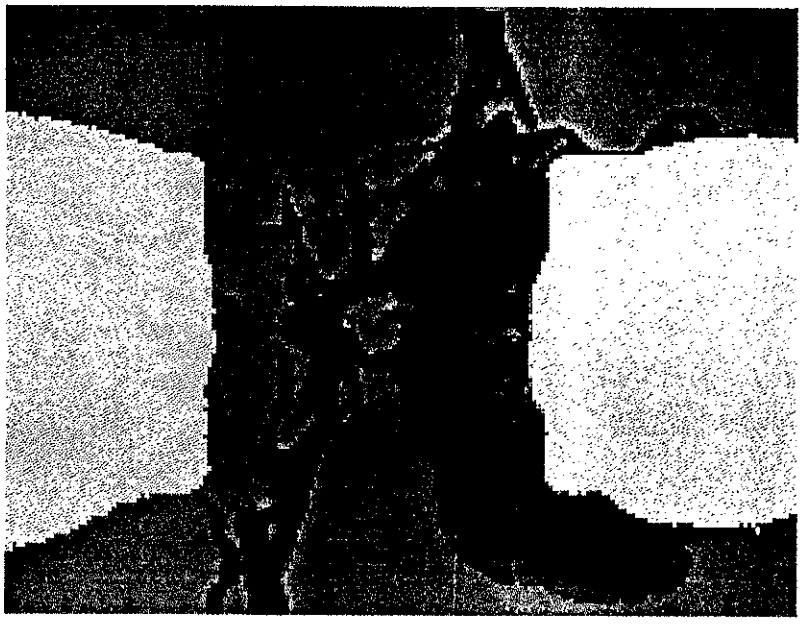

Figure 4.9 Absorption patterns at an applied voltage of 2.75 kV (a) probed at the end of the applied voltage and the corresponding image processed difference photo (b).

(a)

(b)

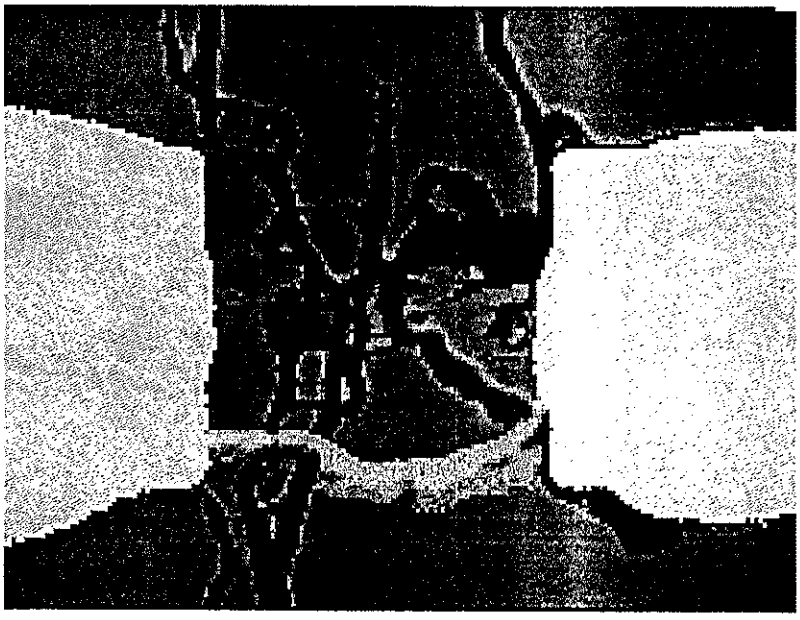

Figure 4.10 Absorption patterns and filament emission when permanent current flow did occur at an applied voltage of 2.75 kV (a) probed 20 ns after laser activation BEFORE the onset of permanent current and the corresponding image processed difference photo (b).

(a)

(b)

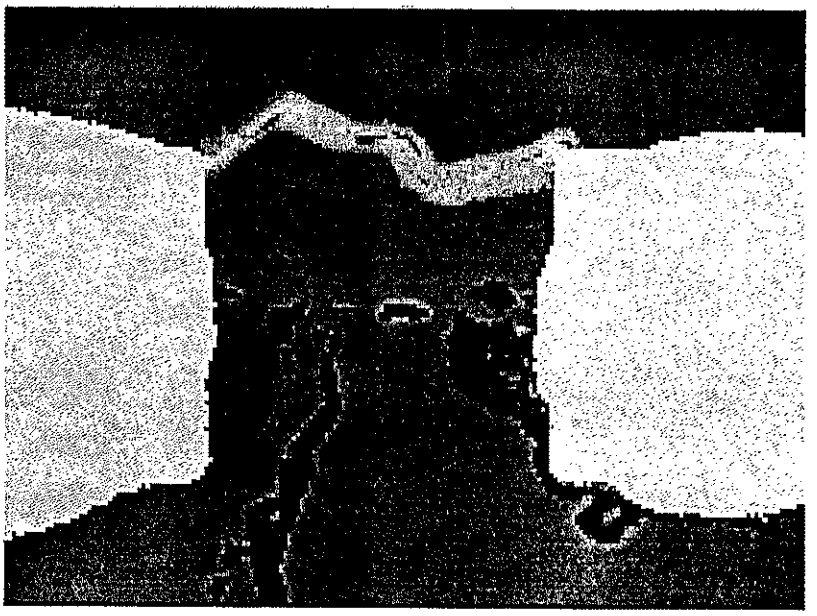

Figure 4.11 Absorption patterns and filament emission when permanent current flow did occur at an applied voltage of 2.75 kV (a) probed 50 ns AFTER the onset of permanent current and the corresponding image processed difference photo (b).

(a)

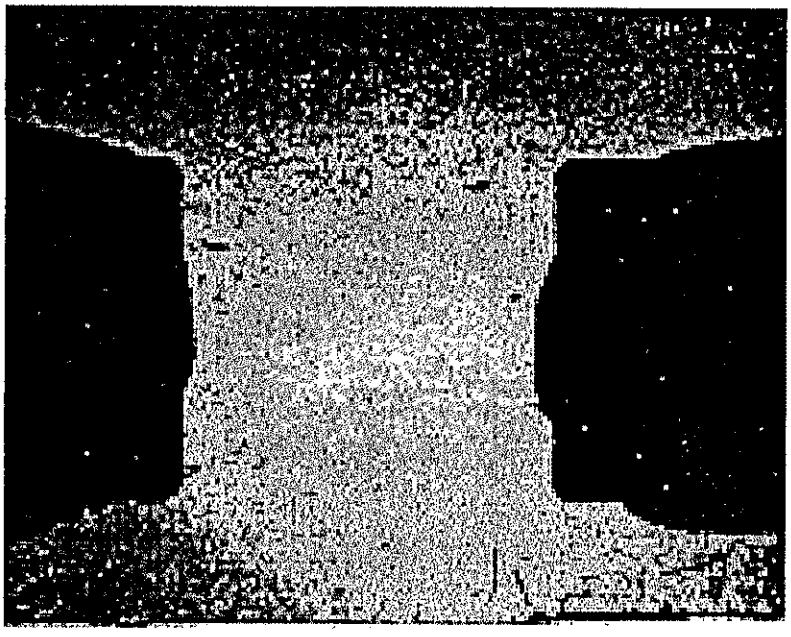

(b)

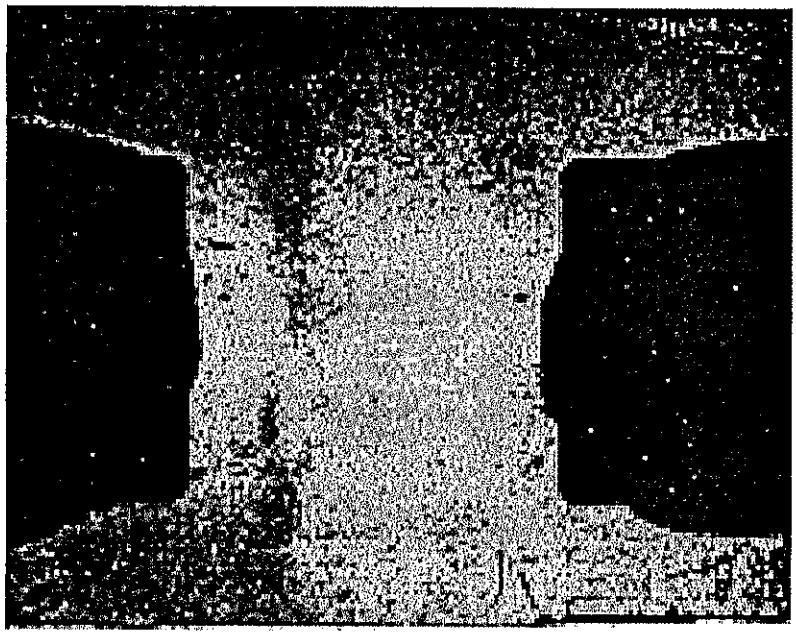

Figure 4.12 Variation of absorption structures with laser activation energy for (a) E = 0 μJ, and (b) E = 0.12 μJ.

(a)

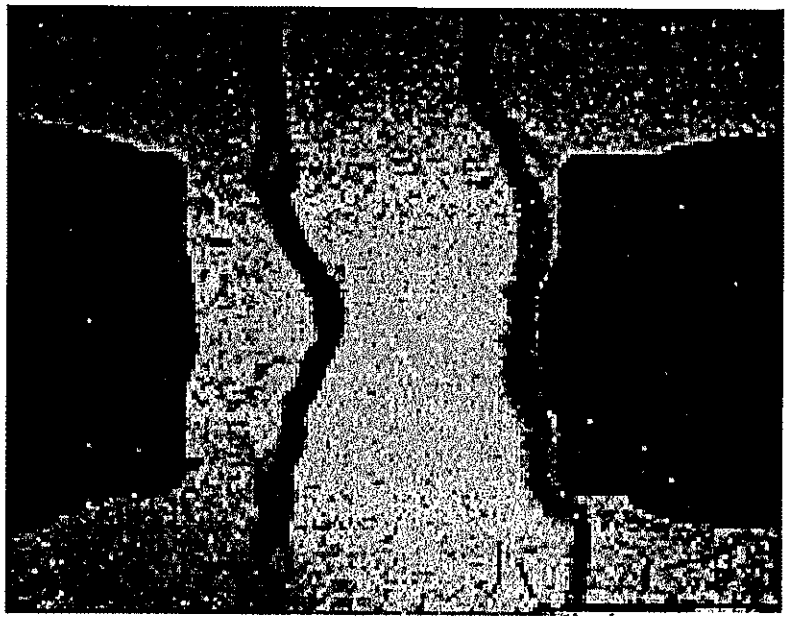

(b)

Figure 4.13 Variation of absorption structures with laser activation energy for (a) E = 0.6 μJ, and (b) E = 5.0 μJ.

(a)

(b)

Figure 4.14 Variation of absorption structures with laser activation energy for (a) E = 24 μJ, and (b) E = 33 μJ.

(a)

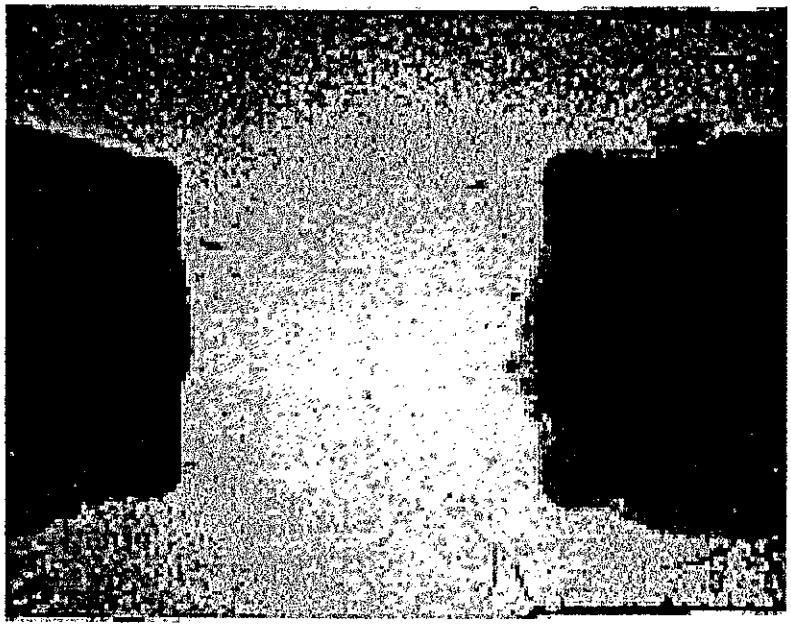

(b)

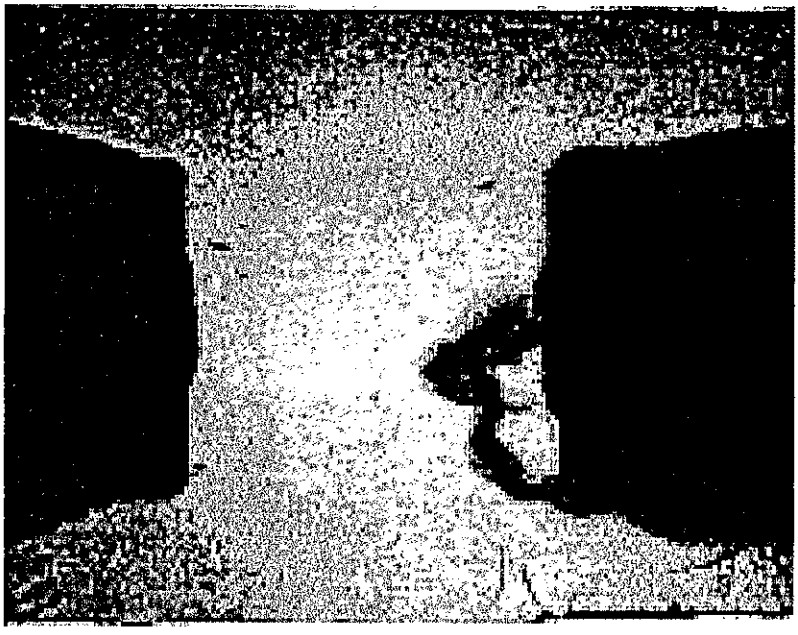

Figure 4.15 Variation of absorption structures with applied voltage for (a) 1.0 kV and (b) 1.5 kV.

(a)

(b)

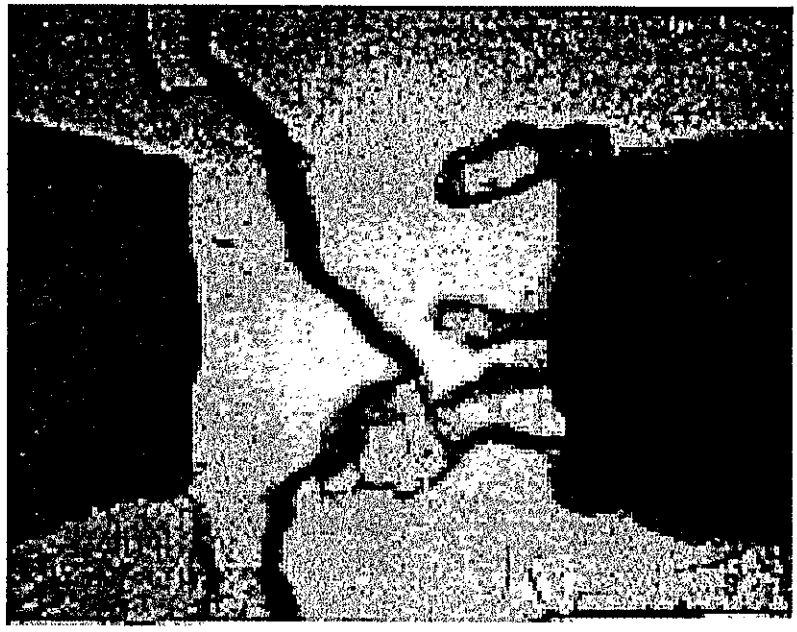

Figure 4.16 Variation of absorption structures with applied voltage for (a) 1.75 kV and (b) 2.0 kV.

(a)

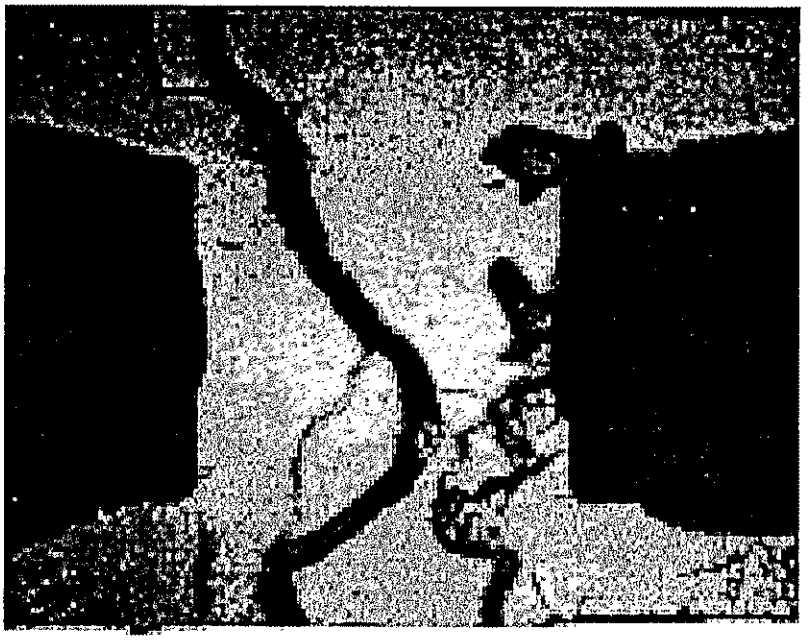

(b)

Figure 4.17 Variation of absorption structures with an applied voltage of 2.5 kV without (a) and with (b) current filament.

CHAPTER 5

DISCUSSION AND CONCLUSION

The electro-absorption measurements on semi-insulating GaAs switches showed for low applied voltage operating in the linear mode, the occurrence of a 100 μm cathode layer with high electric field intensity. The injection of electrons at this contact seems to form mushroom like space charge regions, probably due to trapping of the injected electrons. The relatively small Joule energy in the linear mode GaAs switch is unlikely to cause a temperature change in the cathode area large enough to explain this pattern. The microsecond long decay time of the mushroom like structure (fig. 4.6) is assumed to be due to thermal emission of electrons from deep traps.

At higher voltages absorption bands at both the cathode and the anode are observed after laser activation. Magnitude of fields in the absorption bands exceed 50 kV/cm as shown by calibration measurements. Whereas the cathode layer is voltage dependent (it decays right then the voltage is removed from the switch), the anode structure is current related. In the case of linear switch operation the anode pattern fades away with diminishing current. When permanent current after laser activation is recorded this lock-on current is always connected with the occurrence of at least one filament possibly caused by collisional ionization in the high field domain. The filament is seen to short out the high field regions. Permanent damage due to Joule heating mainly at the contacts but also in regions inside the gap is seen.

due to Joule heating mainly at the contacts but also in regions inside the gap is seen. In order to utilize the lock-on effect but prevent permanent damage the Joule energy in the filaments must be reduced either by shortening the duration of the applied voltage pulse or by distributing the current over an increased number of filaments (multi-channeling).

It has been observed that the threshold for the occurrence of the permanent current can be shifted by varying either the intensity of the activation laser or by the applied voltage. For a fixed illumination intensity, increasing the bias on the switch tended to lower this threshold and cause the switch to go into the permanent current mode. For a fixed voltage bias, increasing the illumination intensity tended to also lower this threshold. The threshold for the occurrence of current filaments was observed to be 900 A/cm^2 but ranged from 880 A/cm^2 to 1000 A/cm^2.

In conclusion, this method of analyzing the field domains in the bulk of photoconductive switches has been shown to be feasible. With further calibration of specific magnitudes with electric field intensities, band-edge absorption imaging could be a practical means of analyzing and optimizing the physical operation of GaAs photoconductive switches.

REFERENCES

1. S.M. Sze, Physics of Semiconductor Devices, J. Wiley & Sons: New York (1981).
2. S.E. Ralph and D. Grishkowsky, *Appl. Phys. Lett.* 59, 1972 (1991).
3. W.R.Donaldson, "Optical Probing of Field Dependent Effects in GaAs Photoconductive Switches," *Proc. 8th IEEE Int. Pulsed Power Conf. (San Diego, CA)*, 45 (1991).
4. R.P.Brinkmann, K.H.Schoenbach, D.C.Stoudt, V.K.Lakdawala, G.A.Gerdin, and M.K.Kennedy, "The Lock-On Effect in Electron-Beam-Controlled Gallium Arsenide Switches," *IEEE Trans. Elect. Dev.* 38, 701 (1991).
5. G.M.Loubriel, W.M.O'Malley, and F.J.Zutavern, "Toward Pulsed Power Uses for Photoconductive Semiconductor Switches: Closing Switches," *Proc. 6th IEEE Pulsed Power Conf. (Arlington, VA)*, 145 (1987).
6. D.C.Stoudt, K.H.Schoenbach, R.P.Brinkmann, V.K.Lakdawala, and G.A. Gerdin, "Optical and Electron-Beam Control of Semiconductor Switches," *IEEE Trans. Elect. Dev.* 37, 2478 (1990).
7. J.S.Kenney, R.J.Allen, S.Ludwig, and K.H.Schoenbach, "The Temporal Development of Instabilities in Low Light Activated GaAs Switches," *Proc. IEEE Power Modulators Conf. (Myrtle Beach, SC)*, (1992).

8. J.L.Pankove, Optical Processes In Semiconductors, Dover Publications Inc., New York (1971), p.22.

9. W. Franz, *Zeitschrift f. Naturfosch.* 13, 484 (1958).

10. L.V. Keldysh, *Sov. Phys. JETP* 7, 788 (1958).

11. J.L.Pankove, Optical Processes In Semiconductors, Dover Publications Inc., New York (1971), p.29.

12. J.L.Pankove, Optical Processes In Semiconductors, Dover Publications Inc., New York (1971), p.47.

13. K. Seeger, Semiconductor Physics, Springer-Verlag, New York (1991), p.324.

APPENDIX A

Quantumechanical treatment of the Franz-Keldysh effect.

The Franz-Keldysh effect is best described as a photon-assisted quantumechanical tunneling through the energy barrier of a band gap. In the presence of an electric field $\mathscr{E}$, the band edges are tilted. An electron moving inside the conduction band a distance x away from the edge and maintaining a constant total energy acquires a kinetic energy $-|e|\mathscr{E}x$ where zero has been assumed at x = 0.

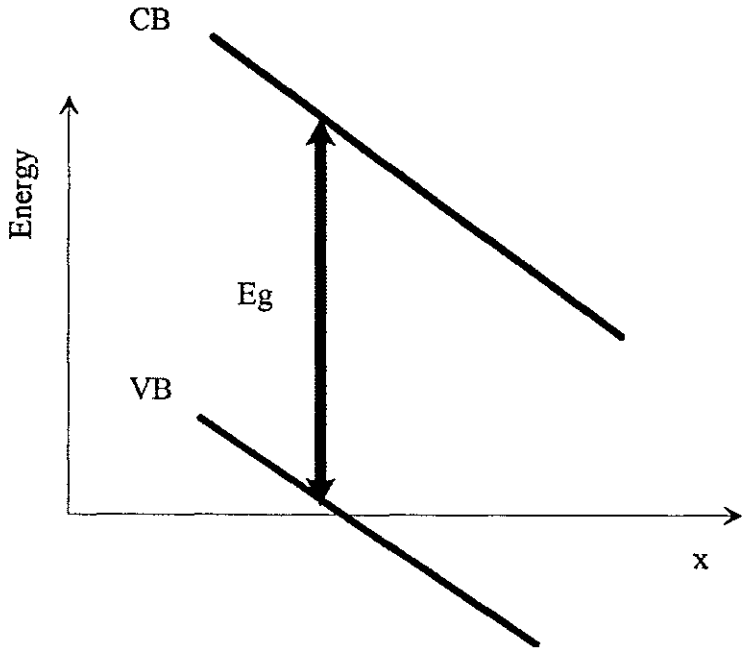

The Schrödinger equation for a quantum mechanical tunneling is equation 1 where the wave function ψ for the electron must be solved. ε is the kinetic energy in the x-direction, where including y and z components $(\hbar^2[k_y^2+k_z^2]/2m_o)$ would give the total kinetic energy.

$$-\left(\frac{\hbar^2}{2m_o}\right)\frac{d^2\psi}{dx^2} - |e|\mathscr{E}x\,\psi = \varepsilon\psi \tag{1}$$

Where: m_o is the rest mass of the electron,

x is the distance travelled,

$\hbar$ is Planck's constant,

$\mathscr{E}$ is the electric field intensity,

ε is the kinetic energy.

For simplification purposes we introduce a new variables ξ which is a linear function of x such that $\xi = ax + b$.

$$x \to \xi = \xi(x) \quad , \qquad \psi(x) \to \psi(\xi(x)) \tag{2}$$

Then by using the following identity we have:

$$\frac{d\psi}{dx} = \frac{d\psi}{d\xi}\xi' \quad , \qquad \frac{d^2\psi}{dx^2} = \frac{d}{dx}\left(\frac{d\psi}{d\xi}\,\xi'\right) = \frac{d^2\psi}{d\xi^2}(\xi')^2 + \frac{d\psi}{d\xi}\,\xi'' \tag{3}$$

The second term is equal to zero ($\xi'' = 0$), and by grouping terms we get:

$$\frac{d^2\psi}{d\xi^2} + \left(\frac{|e|\mathscr{E}x}{\left[\hbar^2/2m_o\right]a^2}\right)\psi = \left(\frac{\varepsilon}{\left[\hbar^2/2m_o\right]a^2}\right)\psi \tag{4}$$

By rearranging and equating coefficients with $\xi = ax + b$ we have:

$$\frac{d^2\psi}{d\xi^2} = -\left[\left(\frac{|e|\mathscr{E}}{\left(\hbar^2/2m_o\right)a^2}\right)x + \left(\frac{\varepsilon}{\left(\hbar^2/2m_o\right)a^2}\right)\right]\psi \tag{5}$$

$$a = -\sqrt[3]{\frac{|e|\mathscr{E}}{\hbar^2/2m_o}}, \qquad b = +\left(\frac{\varepsilon}{|e|\mathscr{E}}\right) a \tag{6}$$

If we introduce an effective length l = 1/a then we have a simplified form for ξ.

$$\xi = -\left(x + \frac{\varepsilon}{|e|\mathscr{E}}\right) / l \tag{7}$$

Now we have a simplified form for our Schrödinger equation. It is a ordinary differential equation of second order which has two independent solutions which are Airy Functions Ai(ξ), and Bi(ξ).

$$\frac{d^2\psi}{d\xi^2} = \xi\ \psi \tag{8}$$

For large positive values of ξ which is valid inside the forbidden gap the solution for ψ is:

$$\psi \propto \xi^{-1/4} \exp\left(\pm\frac{2}{3}\xi^{3/2}\right) \tag{9}$$

Let us denote this expression by y. For a finite electron density ψ has to vanish at infinite values of ξ and only a negative value of the exponent is physically significant for $\xi > 0$. The solution is essentially an exponential decrease with distance from the origin. If we were to consider a conduction electron within the conduction band or the forbidden gap the solution would be correct if we replace the free electron mass by the effective mass.

The probability of finding an electron at x is given by $|\psi(x)|^2 dx$. The absorption coefficient α is then proportional to the probability integrated over the

energy gap as shown.

$$\alpha \propto \int|\psi(\xi)|^2 d\xi \propto \int y^2 d\xi - y^2\xi - (dy/d\xi)^2 \tag{10}$$

The evaluation of this integral is avoided by using some algebraic manipulation and recalling the identity that $\psi \alpha \xi$ so that $d^2y/d\xi^2 = \xi y$ in the following way.

$$y^2 - \left(2y\frac{dy}{d\xi}\xi + y^2\right) - \left(2y\frac{dy}{d\xi}\xi\right) \tag{11}$$

$$\left(2y\frac{dy}{d\xi}\xi + y^2\right) - \frac{d}{d\xi}(y^2\xi) \tag{12}$$

$$\left(2y\frac{dy}{d\xi}\xi\right) - 2\frac{dy}{d\xi}[\xi y] - 2\frac{dy}{d\xi}\left[\frac{d^2y}{d\xi^2}\right] - \frac{d}{d\xi}\left[\left(\frac{dy}{d\xi}\right)^2\right] \tag{13}$$

Then we have:

$$y^2 - \frac{d}{d\xi}\left[\, y^2\xi - (dy/d\xi)^2 \,\right] \tag{14}$$

Substituting this equation back into the integral we have:

$$\alpha \propto \int y(\xi)^2 d\xi - \int \frac{d}{d\xi}[y^2\xi - (dy/d\xi)^2]d\xi - y^2\xi - (dy/d\xi)^2 \tag{15}$$

If we neglect the higher powers of ξ, consider only the exponential dependence and recall the definitions of ξ and l as defined earlier we get the following.

$$\alpha \propto \exp\left(-\frac{4}{3}\xi^{3/2}\right) - \exp\left[-\frac{4}{3}\left(\frac{E_g - \hbar\omega}{|e|\mathscr{E}l}\right)^{3/2}\right] - \exp\left(-\frac{4\sqrt{2m}(E_g - \hbar\omega)^{3/2}}{3|e|\mathscr{E}\hbar}\right) \tag{16}$$

In this approximation x = 0 and $\mathscr{E} = E_g - \hbar\omega$. What we see is that for a given photon energy $\hbar\omega$, the absorption increases with electric field intensity. This can be interpreted as a shift of the absorption edge to lower photon energies.

With some rearranging equation 16 is seen to be the same as equation 2 on page 14. In the exponent the reciprocal of the electric field has a linear dependence. The only difference is in the representation of the energy difference at location x, ($\{E - E_c\}$ vs $\{E_g - \hbar\omega\}$). The resulting energy is essentially the same as shown in the following picture.